Monograph:
Billings, S.A., Guo, L.Z. and Wei, H.L. (2003) Identification of coupled MAP lattice models for spatio-temporal patterns using wavelets. Research Report. ACSE Research Report no. 848 . Automatic Control and Systems Engineering, University of Sheffield

IDENTIFICATION OF COUPLED MAP LATTICE MODELS FOR SPATIO-TEMPORAL PATTERNS USING WAVELETS

S. A. BILLINGS, L. Z. GUO, AND H. L. WEI

Department of Automatic Control and Systems Engineering
University of Sheffield
Sheffield, S1 3JD
UK

Research Report No. 848
October 2003

Identification of coupled map lattice models for spatio-temporal patterns using wavelets

Billings, S. A., Guo, L. Z. and Wei, H. L.

Department of Automatic Control and Systems Engineering
University of Sheffield
Sheffield S1 3JD, UK
FIRST REVISED JUNE 2004
SECOND REVISED OCTOBER 2004

Abstract

This paper introduces a new approach for the identification of coupled map lattice models of complex spatio-temporal patterns from measured data. The nonlinear functionals describing the evolution of the spatio-temporal patterns are constructed using B-spline wavelet and scaling functions. This provides a multiresolution approximation for the underlying spatio-temporal dynamics. An orthogonal least squares algorithm is used to determine the suitable terms from wavelet functions to form an accurate representation of the nonlinear spatio-temporal dynamics. Three examples are used to demonstrate the application of the proposed new approach.

1 Introduction

Complex spatio-temporal patterns have been widely observed and explored in recent years involving diverse fields such as physical, chemical, biological, and ecological systems (Kaneko 1993, Sóle, Valls and Bascompte 1992, Yanagita and Kaneko 1997, Tabuchi, Yakawa and Mallick et al. 2002, Köhler, Reinhard and Huth 2002, Bertram, Beta, Rotermund, and Ertl 2003, Goldman, et al. 2003, Adamatzky 2003). A large number of current studies of pattern formation phenomena involve observing what patterns are formed or changed under a variety of initial and boundary conditions. But an interesting and important question needs to be addressed: if an observed pattern formation follows some dynamical laws, then how can this dynamical origin be revealed effectively? In some instances, the dynamical origin of spatio-temporal pattern formation can be represented as partial differential equations (PDE's). But in many other cases such as for example in ecological systems, only a series of snapshots of the spatial pattern are available. At

the same time, the study of the formation and evolution of spatio-temporal patterns normally requires a model with a specified accuracy. In both cases, however, obtaining or deriving such a dynamical model or PDE describing the pattern formation is by no means straightforward because either the interactions involved are too complex or there may be no established laws on which to base the choice of the model. In this case, it would be advantageous if a model could be identified from the observed patterns. The model could then be used for the analysis of pattern formation or in control.

Computer simulations have emerged as an effective and powerful tool to study complex spatio-temporal patterns. In such cases the spatio-temporal dynamical systems by necessity are discretised in space as well as in time. This was one of the main motivations for the introduction of coupled map lattice (CML) models of spatio-temporal systems. CML models were developed in the late 80's by Kaneko (1985, 1986, 1989a) and can exhibit surprisingly rich dynamical behaviours, including spatio-temporal chaos, intermittency, traveling waves and pattern formation (Kaneko 1989b). CML's have been used to model convected temperature fluctuations in the atmosphere (Platt and Hammel 1997), boiling processes (Yanagita 1992), spatio-temporal chaos in fluid flows (He, Cao and Li 1995) and cloud dynamics (Yanagita and Kaneko 1997). But most of the studies of CML's mainly concentrate on analysing the properties and behaviours of CML's such as chaos. Just like the case of PDE's, the identification of CML models from observations or measured data is still regarded as a very important but difficult problem. The aim of this paper is to introduce a new approach to identifying the local CML equations from spatio-temporal observations using wavelets.

While there are many papers which describe the analysis of the complex and diverse behaviour of known or given CML models, very little research has been done on the identification or reconstruction of CML models from observed spatio-temporal patterns or snapshots. Some methods for the identification of local CML models from spatio-temporal observations have been proposed (Coca and Billings 2001, Mandelj, Grabec and Govekar 2001, Marcos-Nikolaus, Martin-Gonzalez and Sóle 2002, Grabec and Mandeji 1997, Parlitz and Merkwirth 2000). In practice however, some of these approaches may fail to produce models that accurately describe the underlying spatio-temporal patterns either due to an inability to adapt the model structure to that of the unknown system, or because the functions used to implement the model structure are not suitable for modelling the underlying dynamics. This is especially critical when an equivalent description of real-world systems is sought. In such cases the estimated model should provide very accurate information regarding the dynamical properties of the observed system. Theoretical studies have shown that the wavelet representation of any nonlinear function can be shown to be asymptotically near optimal in the sense that the convergence rates are equal to the best attainable using general nonlinear approximation schemes (DeVore, Jawerth, and Popov 1992). In addition wavelet approximations also provide similar rates of approximation for functions belonging to a wide variety of function spaces including functions with sparse singularities or functions that are not uniformly smooth or regular. All these properties suggest that wavelet multiresolution expansions should provide an excellent foundation for the development of identification algorithms for nonlinear CML models.

A mixed wavelet and NARX approach to the identification of nonlinear spatio-temporal dynamical systems has been discussed in Billings, Wei, Mei, and Guo (2003). In this paper, wavelets,

as regressors, are directly used to identify the CML models, which drive spatio-temporal pattern formation, from measured data or snapshots for the purpose of revealing the dynamical origin of the given patterns. The nonlinear functionals describing the evolution of the spatio-temporal patterns are constructed using B-spline wavelet and scaling functions, originally introduced by Chui and Wang (1991). The orthogonal least squares algorithm proposed by Chen, Billings, and Luo (1989) is used to determine the suitable terms from B-spline wavelet and scaling functions. The paper is organised as follows. Section 2 introduces the CML model of spatio-temporal dynamical systems. The wavelet models are introduced in section 3 including an introduction to wavelets and a discussion about wavelet model structures. In section 4, the identification method and the implementation strategy are presented. Section 5 illustrates the proposed approach using three examples. Finally conclusions are drawn in section 6.

2 The CML model

Consider a d-dimensional lattice I consisting of the set of all integer coordinate vectors $i = (i_1, \cdots, i_d) \in \mathbf{Z}^d$. The deterministic CML state-space model of spatio-temporal dynamical systems defined over I is of the following form (Coca and Billings 2001)

$$x_i(t) = f_l(x_i(t-1), u_i(t-1)) + f_c(x_i(t-1), u_i(t-1), \mathbf{s}^m x_i(t-1), \mathbf{s}^m u_i(t-1)) \tag{1}$$

where $x_i(t) \in X_i \subset \mathbf{R}^n$ and $u_i(t) \in U_i \subset \mathbf{R}^l$, X_i and U_i are open sets, n and l-dimensional vectors representing the local state and input variables respectively at the ith site in I, and f_l and f_c are piecewise differentiable maps. $\mathbf{s}^m$ is a spatial shift operator, which is defined as

$$\mathbf{s}^m = (s^{p_1}, s^{p_2}, \cdots, s^{p_m}) \tag{2}$$

such that

$$\mathbf{s}^m x_i(t) = (s^{p_1} x_i(t), s^{p_2} x_i(t), \cdots, s^{p_m} x_i(t)) = (x_{i+p_1}(t), x_{i+p_2}(t), \cdots, x_{i+p_m}(t)) \tag{3}$$

where $p_1, p_2, \cdots, p_m$ are the indices of the neighbours of the ith site - that is the region in I around the ith site, which influences the dynamics of that particular site.

The CML model (1) can also be written, in terms of the global state and input variables $x = \{x_i\}_{i \in I} \subset X = \prod_{i \in I} X_i$ and $u = \{u_i\}_{i \in I} \subset U = \prod_{i \in I} U_i$, as follows

$$x(t) = f(x(t-1), u(t-1)) \tag{4}$$

where $f : X \times U \to X$ is the function sequence $f = \{f_i\}_{i \in I}$ with $f_i = f_l + f_c$ and $i = \{i_1, \cdots, i_d\} \in I$.

In general, the direct measurement of the state vector x is not possible and only some observable variable y which depends on the state and input can be measured. Therefore, the state-space model of the CML is usually complemented with a measurement equation

$$y_i(t) = h_i(x(t)) \tag{5}$$

Here it is assumed that the lattice equations are spatially invariant over the observed spatial domain. This implies that the difference equations corresponding to each lattice site or location are the same for all lattice sites. Generally it is also assumed that the following input-output representation

$$y_i(t) = g(\mathbf{q}^{n_y} y_i(t), \mathbf{q}^{n_u} u_i(t), \mathbf{s}^{m'} \mathbf{q}^{n_y} y_i(t), \mathbf{s}^{m'} \mathbf{q}^{n_u} u_i(t)) \tag{6}$$

can be derived for any site from (1) and (5). In (6), $\mathbf{q}$ is a backward shift operator such that

$$\mathbf{q}^{n_y} y_i(t) = (y_i(t-1), y_i(t-2), \cdots, y_i(t-n_y)) \tag{7}$$

A number of sufficient conditions which ensure that this can be found are given in Billings and Coca (2002) and Guo, Mei and Billings (2002).

Many spatio-temporal patterns can be generated from the above CML model (6). Two typical examples are systems which can be described by the wave equation and predator-prey populations in ecosystems. CML models of both types of systems will be identified using the proposed method later on in this paper.

Note that in eqn. (6) g is generally a nonlinear differential map depending on the history of local input and output variables, and on the variables at some neighbouring sites. If g is unknown then the nonlinearity of g makes it difficult to apply traditional identification techniques. It is common practice to approximate nonlinear input-output equations from the available data using a known set of basis functions or regressors. Typical classes of regressors used in nonlinear identification include polynomial and rational functions, Gaussian radial basis functions and wavelets. In this paper, wavelets are chosen as basis functions to approximate the CML model (6).

3 Wavelet models

3.1 Wavelets for identification

The approximating properties of wavelet multiresolution expansions in many situations outperform many other approximation schemes (DeVore et al. 1992). Because of the space-frequency localisation properties of the functions involved, wavelets are ideal candidates to represent spatial model structures which can match the complexity of the underlying nonlinear relationship

without the risk of overfitting. The advantage in this case is that the approximation can be refined locally over a subregion in the input domain without affecting the model elsewhere too much.

In practice, a multiresolution approximation can be implemented using different types of wavelet and scaling basis functions, the class usually depends on the applications. For nonlinear system identification, the class of semi-orthogonal wavelet multiresolution approximation introduced by Chui and Wang (1992), defined in terms of B-spline scaling and wavelet basis functions are particularly suitable. The main reasons are that B-spline wavelets are compactly supported and analytic which provide near-optimal time-frequency localisation. Moreover, a comparative study of the approximation power of some classes of wavelet decompositions (Sweldens and Piessens 1994) emphasized that B-spline wavelets are by far the best in terms of the approximation rate. Practically this means that fewer resolution levels are required to approximate a function with a given degree of accuracy. Since each extra level doubles the amount of work, the selection of wavelets is clearly important.

3.2 B-spline wavelet models

Consider a wavelet multiresolution approximation structure which allows the representation of a square-sumable function $f(\cdot)$ as a series expansion in terms of the translates and dilates of a scaling and a wavelet basis function $\phi(x)$ and $\psi(x)$

$$f(x) = \sum_k c_{j,k}\phi_{j,k}(x) + \sum_{l=j}^{\infty}\sum_k d_{l,k}\psi_{l,k}(x) \tag{8}$$

where $c_{j,k}$ and $d_{l,k}$ are the coefficients of the expansion, $\phi_{j,k}(x) = 2^{j/2}\phi(2^j x - k)$ and $\psi_{l,k}(x) = 2^{l/2}\psi(2^l x - k)$. In (8) j is an integer representing the scale while k is the translation parameter, an integer indicating the location of the basis function.

The scaling basis function considered in this paper is the m-th order cardinal B-spline function $\phi(x) = \phi^m(x) = \beta^m(x)$ given by the recursive relation

$$\beta^m(x) = \frac{x}{m-1}\beta^{m-1}(x) + \frac{m-x}{m-1}\beta^{m-1}(x-1) \tag{9}$$

where $\beta^1(x)$ is the indicator function

$$\beta^1(x) = \begin{cases} 1 & \text{if } x \in (0,1) \\ 0 & \text{otherwise} \end{cases} \tag{10}$$

The wavelet function is defined as a linear combination of scaling functions

$$\psi^m(x) = \sum_{l=0}^{3m-2} q_l \phi^m(2x-l) \tag{11}$$

with the coefficients given by

$$q_l = \frac{(-1)^l}{2^{m-1}} \sum_{k=0}^{m} \left(\begin{array}{c} m \\ k \end{array} \right) \phi^{2m}(l-k+1),\ l = 0, \cdots .3m-2 \tag{12}$$

The wavelet model of the input-output CML equation (6) can be obtained by expanding the nonlinear function g as a multiresolution wavelet series in terms of the B-spline scaling and wavelet functions as follows

$$y_i(t) = g(X) = \sum_{j,k} \theta_{j,k} g_{j,k}(X), j, k \in \mathbf{Z} \tag{13}$$

where

$$X = (\mathbf{q}^{n_y} y_i(t), \mathbf{q}^{n_u} u_i(t), \mathbf{s}^{m'} \mathbf{q}^{n_y} y_i(t), \mathbf{s}^{m'} \mathbf{q}^{n_u} u_i(t)) \tag{14}$$

is the vector of regression variables consisting of past outputs, inputs, coupling variables from the neighbouring sites, $\theta = \{\theta_{j,k}, j, k \in \mathbf{Z}\}$ is the parameter vector and $g = \{g_{j,k}\}_{j,k \in \mathbf{Z}}$ represents the model set, the family of scaling and wavelet basis functions (or regressors) doubly indexed according to scale and location.

Note that if $X = x$ is a scalar, then

$$\{g_{j,k}(x)\} = \{\phi_{j_0,k}(x), \psi_{j,k}(x)\}, j \geq j_0, j, k \in \mathbf{Z} \tag{15}$$

where $\phi(x) = \phi^m(x) = \beta^m(x)$ and $\psi(x) = \psi^m(x)$ for some positive integer m are the B-spline scaling and wavelet functions given in (9) and (11) and j_0 is the starting scale. Multi-variable bases can be constructed using the tensor product method. A $d-$ dimensional multi-resolution approximation can be implemented using the basis functions $\{\Phi(x)\}$ and $\{\Psi^{(l)}(x)\}_{l=1,\cdots,2^d-1}$ constructed as tensor products of scalar basis functions. Assuming $X = \{x_1, x_2\}$ for example, the multiresolution decomposition can be implemented in terms of the translation and dilations of the following two-dimensional basis functions

$$\Phi(X) = \phi(x_1)\phi(x_2) \tag{16}$$

$$\Psi^{(1)}(X) = \phi(x_1)\psi(x_2) \tag{17}$$

$$\Psi^{(2)}(X) = \psi(x_1)\phi(x_2)$$

$$\Psi^{(3)}(X) = \psi(x_1)\psi(x_2)$$

In this case

$$\{g_{j,k}(X)\} = \{\Phi_{j_0,k}(X), \Psi^{(1)}_{j,k}(X), \Psi^{(2)}_{j,k}(X), \Psi^{(3)}_{j,k}(X)\}, j \geq j_0, j, k \in \mathbf{Z} \tag{18}$$

4 Identification algorithm

In theory, the wavelet multiresolution approximation is an infinite series expansion. In practice, however, it is not realistic to use all the terms in this infinite series expansion. Generally the objective of the identification algorithm is to obtain a truncated finite representation containing the terms up to some orders of scaling and dilation. Therefore the identified CML model will be an approximate representation of the underlying spatio-temporal dynamics, which can be equivalently described as an infinite wavelet series. Although this is a finite approximation representation, in practice, it can be made to approximate the underlying dynamics at any given accuracy. Note that the series in a truncated space are those up to some dyadic level, which may possibly be infinite because there is no limitation on the translation operation. In practice, the range of measured data is always finite so that there are only finite numbers of translation operations which produce non-empty intersections with the range of data. Therefore, the identified wavelet series are always finite. Furthermore, in many applications, a 3-truncated space is often enough to obtain a good approximation result because the wavelets with higher dyadic level are most likely to have compact support which contains no data points.

The key task of the identification algorithm is to select the desirable terms for the final representation from a given set of candidate terms $\{g_{j,k}(X)\}_{j,k\in\Omega}$. In this paper, the orthogonal least squares algorithm (Chen, Billings, and Luo 1989) is employed to implement the selection task. Based on the algorithm, the iterative identification procedure can be outlined as follows

Step 1 Determine the spatial neighbourhood sites (represented by $\mathbf{s}^{m'}$) of the ith site.

Step 2 Select the time lags n_y and n_u, then the process variables involved in the identification is

$$\{\mathbf{s}^{m'}y_i(t-1), \cdots, \mathbf{s}^{m'}y_i(t-n_y), \mathbf{s}^{m'}u_i(t-1), \cdots, \mathbf{s}^{m'}u_i(t-n_u)\} \tag{19}$$

For above each process variable initialise the following parameters

- the order of B-spline wavelet and scaling functions used to implement the model;
- the starting resolution;
- the number of resolutions.

Step 3 Apply the orthogonal least squares algorithm to obtain the terms and parameters of the CML model (wavelets as regressors).

Step 4 Apply model validity tests to evaluate the model. If no valid models are found, then the set of candidate terms is refined in the following way

- select the resolution just one order higher than that currently used;
- increase the order of B-spline functions;
- add higher dimensional terms to the set of candidate terms.

If data is available from more sensors than the minimum required to extract the CML equations, the additional measurements can be used in model validation. The CML model identified using a set of data from a given spatial site can be validated on data recorded at different spatial locations by computing the model predicted output

$$\hat{y}_j(t) = \tilde{g}(\mathbf{q}^{n_y}\hat{y}_j(t), \mathbf{q}^{n_u}u_j(t), \mathbf{s}^{m'}\mathbf{q}^{n_y}\hat{y}_j(t), \mathbf{s}^{m'}\mathbf{q}^{n_u}u_j(t)) \tag{20}$$

Model predicted output is a much more rigorous test than the one step ahead predicted outputs which most authors use. Note that the one step ahead predicted output is calculated as follows

$$\hat{y}_j(t) = \tilde{g}(\mathbf{q}^{n_y}y_j(t), \mathbf{q}^{n_u}u_j(t), \mathbf{s}^{m'}\mathbf{q}^{n_y}y_j(t), \mathbf{s}^{m'}\mathbf{q}^{n_u}u_j(t)) \tag{21}$$

and includes the measured output on the right hand side which effectively limits the accumulation of errors during iteration. However, the model predicted output eqn.(20) involves only the predicted output terms on the right hand side so that any model errors will quickly accumulate.

Note that in the above identification procedure, the spatial neighbourhood sites (represented by $\mathbf{s}^{m'}$) of the identified site and the time lags (n_y, n_u) need to be known *a priori*. In other words, the neighbourhood of the identified site, that is, the region around that site which influences the dynamics of that site in the spatial domain and the time domain need to be known before starting the identification. In practice, these two factors are important in determining the spatio-temporal dynamics of the underlying system. Determining which site and what time lag should be included in the model structure is therefore very important in CML identification. This problem has been studied by Guo, Mei, and Billings (2002), in which the approach to detect the optimal neighbourhood can be outlined as two steps: first extracting the main features of the underlying spatio-temporal system by thresholding to form a binary counterpart; then applying cellular automata neighbourhood detection algorithms (Mei, Billings, and Guo 2004) to obtain an initial estimate of the neighbourhood. The idea behind the approach is to identify from the data by investigating the gradients of the system output along a variable, say, $y_{i+1}(t-2)$. If the gradient of the system output along this variable is not zero, then $i+1$ is a spatial neighbour and 2 is a significant time lag.

5 Simulation studies

5.1 Example 1 - Non-homogeneous wave equation

Consider the following non-homogeneous wave equation

$$\frac{\partial^2 v(t,x)}{\partial t^2} - C\frac{\partial^2 v(t,x)}{\partial x^2} = u(t,x), x \in [0,1] \tag{22}$$

with initial conditions

$$\begin{aligned} v(0,x) &= 0 \\ \frac{dv(0,x)}{dt} &= 4\exp(-x) + \exp(-0.5x) \end{aligned} \tag{23}$$

where

$$u(t,x) = -13\exp(-x)\cos(1.5t) - 9.32\exp(-0.5x)\cos(2.1t) \tag{24}$$

For $C = 1.0$ the exact solution $v(t,x)$ of the initial value problem (22), (24) is

$$\begin{aligned} v(t,x) &= 4\exp(-x)\cos(1.5t) + 2\exp(-0.5x)\cos(2.1t) \\ &\quad -4\exp(-x)\exp(-t) - 2\exp(-0.5x)\exp(-0.5t) \end{aligned} \tag{25}$$

The measurement function was taken as

$$y(t,x) = v(t,x) \tag{26}$$

Note that the measurement function is set to be the identity for the purpose of simplicity, but this does not mean the results are trivial because only the input-output behaviours are of interest in the paper.

The reference solution was sampled at 21 equally spaced points over the spatial domain $\Omega = [0,1], x = \{x_1, \cdots, x_{21}\}$. From each location, 500 input/output data points sampled at $\Delta t = \pi/100$ were generated. Note that all data were normalised to the interval $(0,1)$. The data are plotted in Fig.(1).

In this simulation, the neighbourhood was selected to be $i-1$ and $i+1$ in the spatial domain and $t-1, t-2$ in the time domain. A set of 350 observations randomly selected among the data set was used for identification, which is shown in Fig.(2). In addition, 350 input and output data $u_i(t), y_{i-1}(t)$ and $y_{i+1}(t)$ from neighbouring locations $i-1, i+1$ acted as inputs during the identification. The identified model using the orthogonal least squares algorithm with the following parameters: order of B-spline 2, initial scale 0, the maximal resolution 2 for all variables and the tolerance 10^{-5}, are listed in Table (1), where ERR denotes the Error Reduction Ratio (Chen, Billings, and Luo 1989) and STD denotes the standard deviations.

Terms	Estimates	ERR	STD
$\phi_{0,0}(y_i(t-1))$	5.2872e-01	9.9962e-01	1.0031e-02
$\phi_{0,0}(y_{i+1}(t-1))$	5.7757e-01	6.2841e-05	9.1564e-03
$\phi_{0,0}(y_{i+1}(t-2))$	-1.3408e-01	5.7821e-05	8.2893e-03
$\phi_{0,0}(y_{i-1}(t-1))$	4.8932e-01	1.6309e-05	8.0249e-03
$\phi_{0,0}(y_{i-1}(t-2))$	-2.6241e-01	3.1919e-05	7.4801e-03
$\psi_{0,-2}(y_i(t-1))$	1.6730e-01	4.7059e-06	7.3962e-03
$\phi_{0,0}(y_i(t-2))$	-1.9958e-01	4.3115e-06	7.3186e-03
$\psi_{2,0}(u_i(t-1))$	1.6508e-03	2.7065e-06	7.2694e-03
$\psi_{2,2}(y_{i+1}(t-1))$	-1.7741e-01	2.2198e-06	7.2288e-03
$\psi_{1,-2}(y_i(t-1))$	1.4794e-01	1.8533e-06	7.1947e-03
$\psi_{2,3}(y_i(t-2))$	1.6121e-01	1.8011e-06	7.1614e-03
$\psi_{2,2}(u_i(t-2))$	1.4767e-01	1.7555e-06	7.1288e-03
$\psi_{2,3}(y_{i+1}(t-2))$	1.4911e-01	1.6431e-06	7.0982e-03
$\psi_{2,3}(y_{i-1}(t-2))$	-1.3551e-01	1.7367e-06	7.0657e-03
$\phi_{0,-1}(y_{i+1}(t-2))$	-1.2632e-01	1.3398e-06	7.0405e-03

Table 1: Example 1: The terms and parameters of the final CML model

The model predicted output of the identified model is plotted in Fig.(3). Fig.(4) shows the model predicted error between the exact solution and the identified CML model predicted output. The presented results clearly indicate that the error falls in between -0.0171 and 0.0195 and does not grow much in time. The largest error 0.0195 occurs at the 379th time instant at spatial location x_5. The root-mean-square (RMS) of the error is 0.0063. Furthermore, it is observed that there are larger errors around the peaks and valleys. This is to be expected and may be explained from the wavelet compression point of view. Generally there will be significant wavelet coefficients where the signal varies significantly and small coefficients where the signal does not vary too much. In this example, the obtained CML model can be considered as an estimated and compressed version of the real wavelet representation of the original dynamics. Although there are errors between the real output and the model predicted output it is clearly observed that the identified CML model is able to reproduce the original patterns with very high fidelity.

The obtained wavelet coefficients can also be interpreted according to a time-frequency analysis. For instance, the terms $\phi_{0,0}(y_i(t-1))$, $\psi_{0,-2}(y_i(t-1))$ and $\psi_{1,-2}(y_i(t-1))$ in the final model represent three concentrated areas of energy of the signal along the variable $y_i(t-1)$ which indicates the signal has a type of low pass property along $y_i(t-1)$.

5.2 Example 2 - Predator-prey populations in ecosystems

Consider the following spatio-temporal evolution of interacting populations on a two-dimensional coupled map lattice (Sóle, Valls and Bascompte 1992, Coca and Billings 2001)

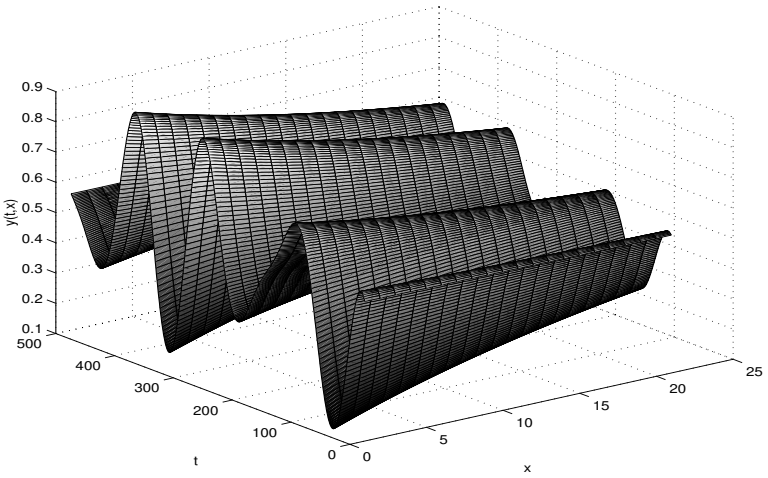

Figure 1: Example 1: System output

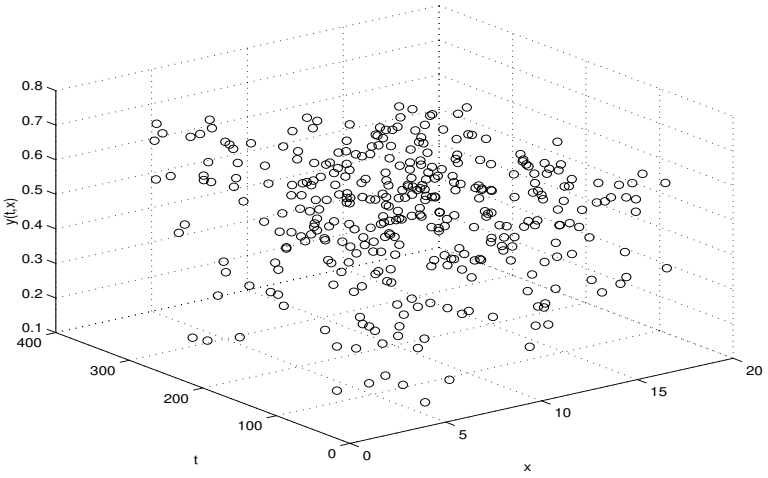

Figure 2: Example 1: The data for identification

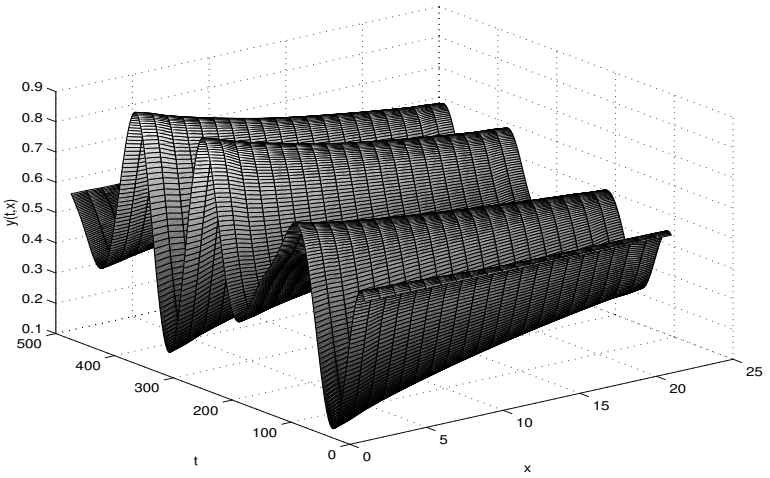

Figure 3: Example 1: Model predicted output

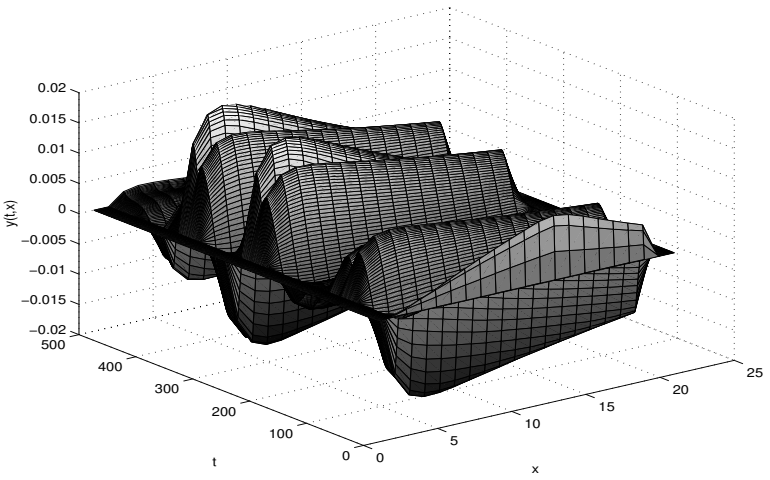

Figure 4: Example 1: Model predicted output

$$
\begin{aligned}
x_i(t) &= \mu x_i(t-1)(1-x_i(t-1))\exp(-\beta y_i(t-1)) + D_1\nabla^2 x_i(t-1) \\
y_i(t) &= x_i(t-1)(1-\exp(-\beta y_i(t-1))) + D_2\nabla^2 y_i(t-1)
\end{aligned} \tag{27}
$$

which $i = (i_1, i_2) \in Z^2$ and the coupling is given by a discrete diffusion operator, i.e.

$$
\begin{aligned}
\nabla^2 x_{i_1,i_2} &= x_{i_1-1,i_2} + x_{i_1+1,i_2} + x_{i_1,i_2-1} + x_{i_1,i_2+1} - 4x_{i_1,i_2} \\
\nabla^2 y_{i_1,i_2} &= y_{i_1-1,i_2} + y_{i_1+1,i_2} + y_{i_1,i_2-1} + y_{i_1,i_2+1} - 4y_{i_1,i_2}
\end{aligned} \tag{28}
$$

This CML model describes the evolution of the host and parasitoid population on the lattice Z^2 in which $x_i = x_{i_1,i_2}$ and $y_i = y_{i_1,i_2}$ are the host and parasitoid population respectively. It has been shown (Sóle, Valls and Bascompte 1992) that this CML model is able to exhibit many interesting spatio-temporal patterns including spiral waves, chaotic and periodic dynamics under the different parameters and/or different initial conditions.

In this simulation, the measurement function used for identification was just set to be $x_i(t)$ and $y_i(t)$ for each site $i \in Z^2$ and the data used for identification was generated by simulating the CML model (27) with $\mu = 4, \beta = 5, D_1 = 0.0001, D_2 = 0.20$ for 100 steps over a 50×50 lattice I starting from randomly generated initial populations and periodic boundary conditions. The data are shown in Figs.(5) and (6). The identification was performed using the proposed method from a set of 100 observation pairs among the data and the four nearest neighbours, namely $(i-1, j), (i+1, j), (i, j-1), (i, j+1)$. Because two subsystems need to be identified (one for x and the other for y), an extra 100 output data $y_i(t)$ for $x_i(t)$ or $x_i(t)$ for $y_i(t)$ from the other subsystem acted as an additional input during the identification. The time lag was set to be 1. The starting resolution was set to be 0 for all variables and the maximal resolutions were set to 2, 1, and 0 for uni, bi, and tri-variates, respectively. The univariate B-spline function of order 3 was used to generate all the higher-dimensional terms by tensor products. It follows that the total number of terms in the set of candidate model set for all two subsystems is 12833. The identified models for each subsystem are listed in Table (2)

The model predicted outputs for two subsystems are plotted in Figs.(7) and (8), respectively. Figs. (9) and (10) show snapshots of the model predicted errors at time instants 1, 10, 50 and 100 between the system outputs and model predicted outputs, which show that the identified CML model can reproduce the spatio-temporal patterns of the original system very well. The RMS's for these snapshots are RMS(x,10) = 0.0031, RMS(x,50) = 0.0034, RMS(x,100) = 0.00093309, RMS(y,10) = 0.00083510, RMS(y,50) = 0.00099306, RMS(y,100) = 0.0010, respectively.

5.3 Example 3 - Two dimensional reaction-diffusion equations

Consider the following two dimensional reaction-diffusion equations (Ramos 1997)

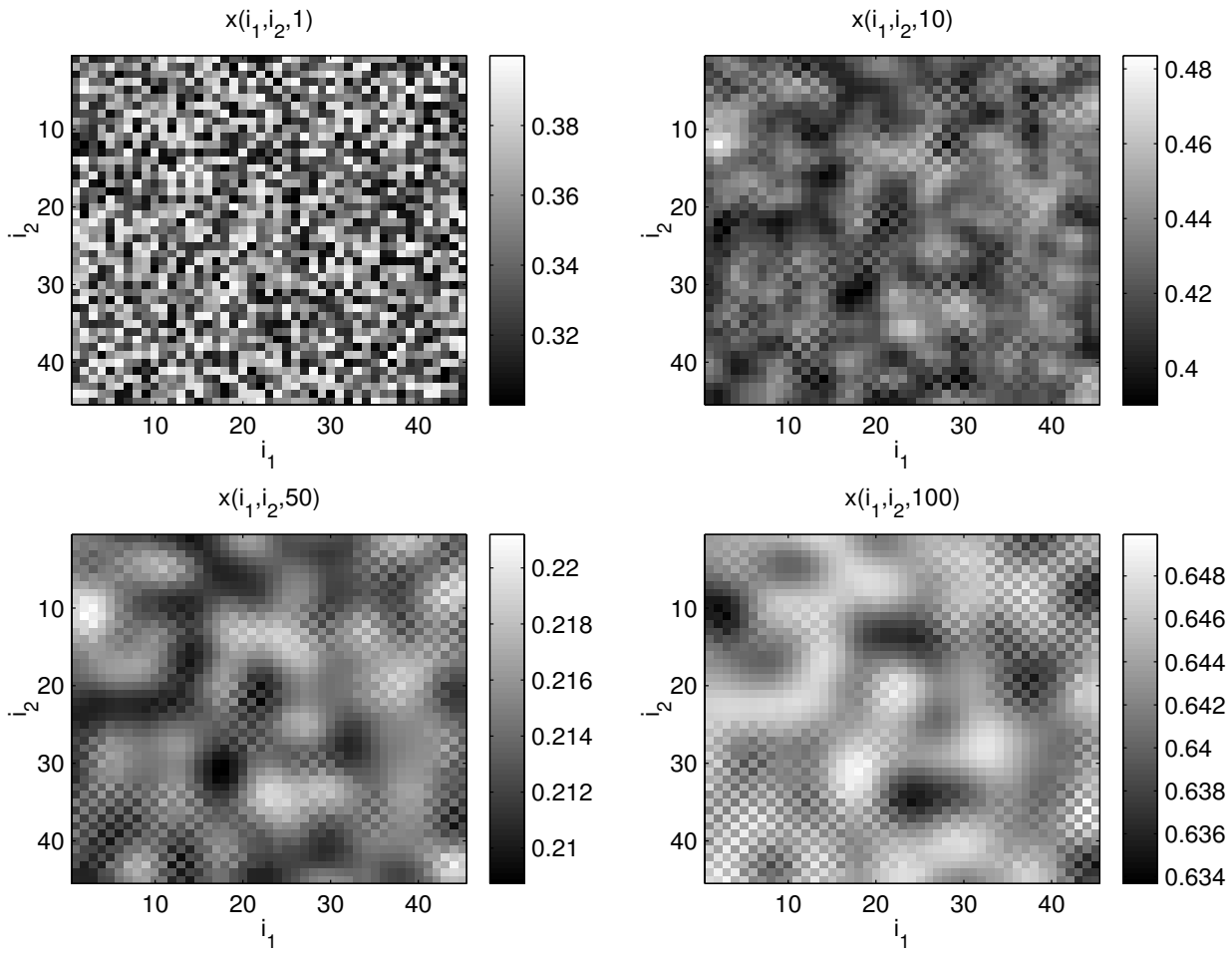

Figure 5: Example 2: Some snapshots of data (x)

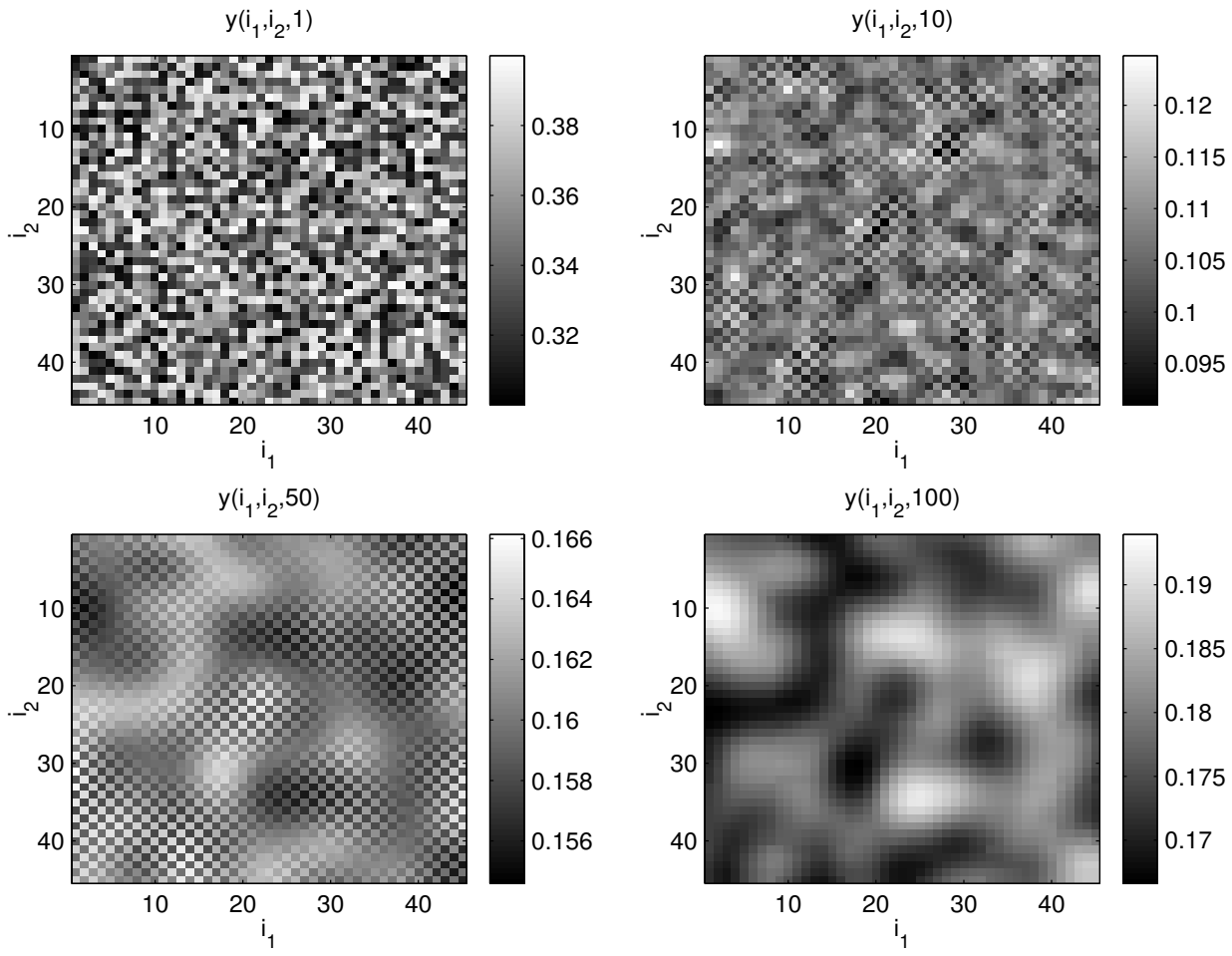

Figure 6: Example 2: Some snapshots of data (y)

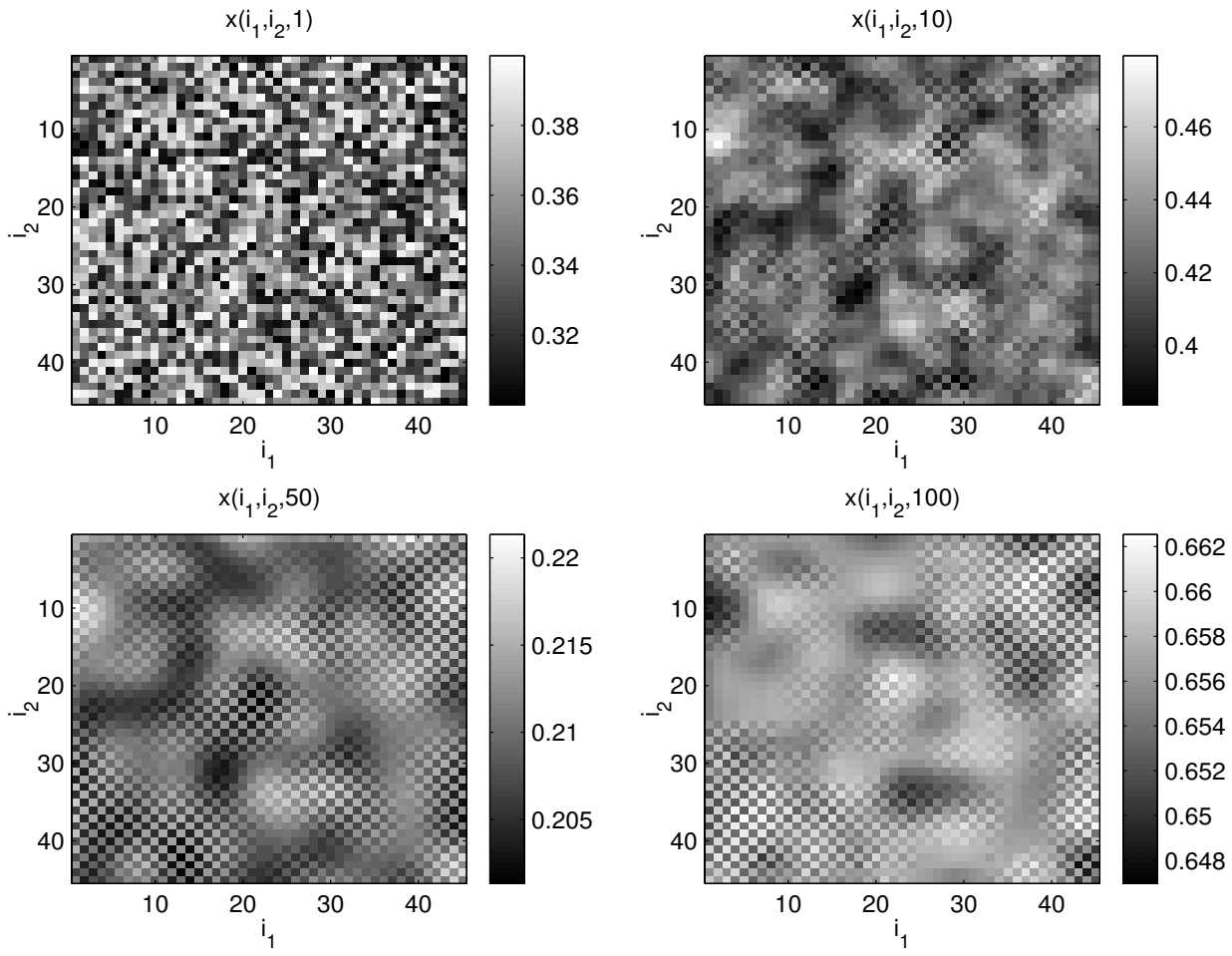

Figure 7: Example 2: Some snapshots of model predicted outputs (x)

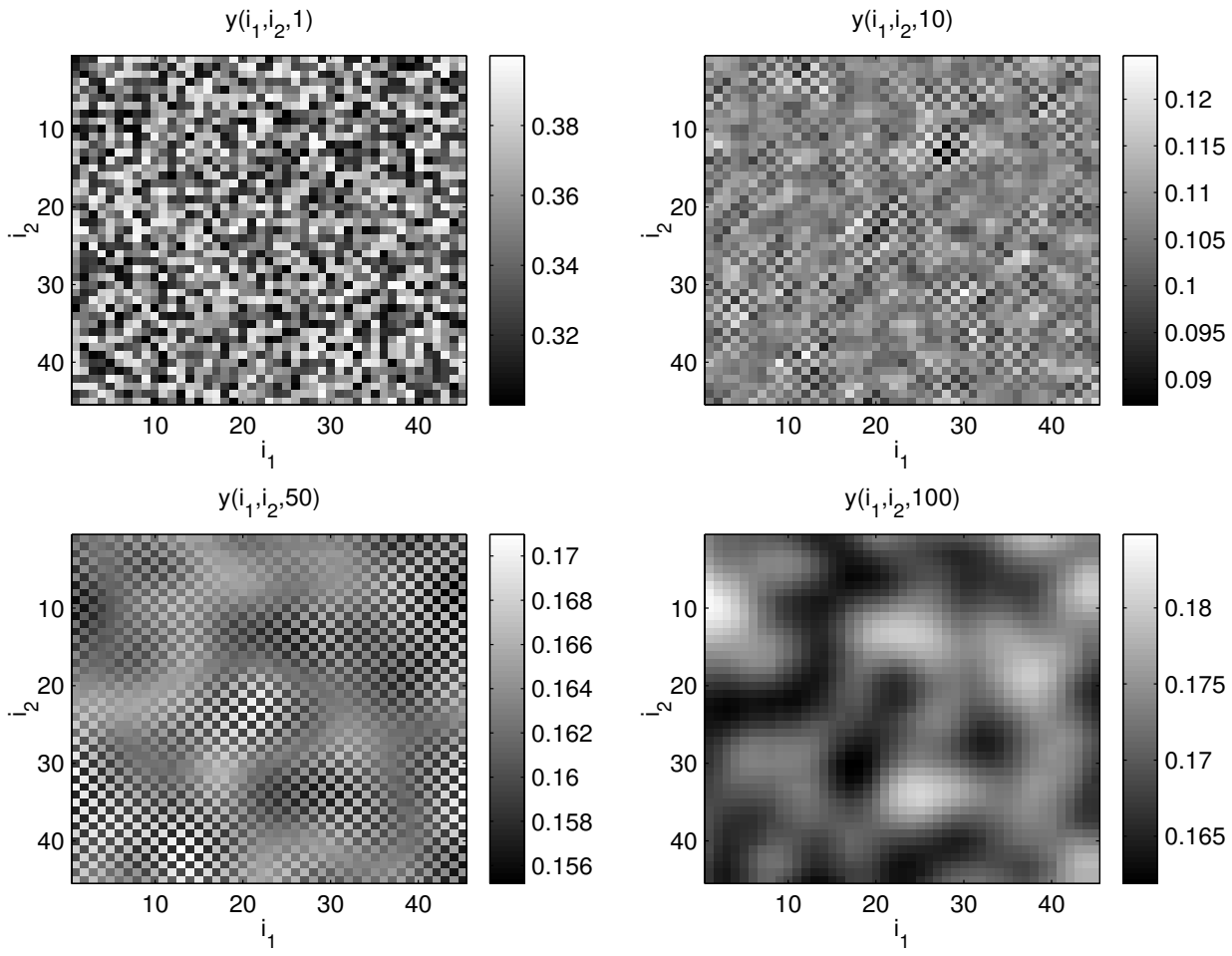

Figure 8: Example 2: Some snapshots of model predicted outputs (y)

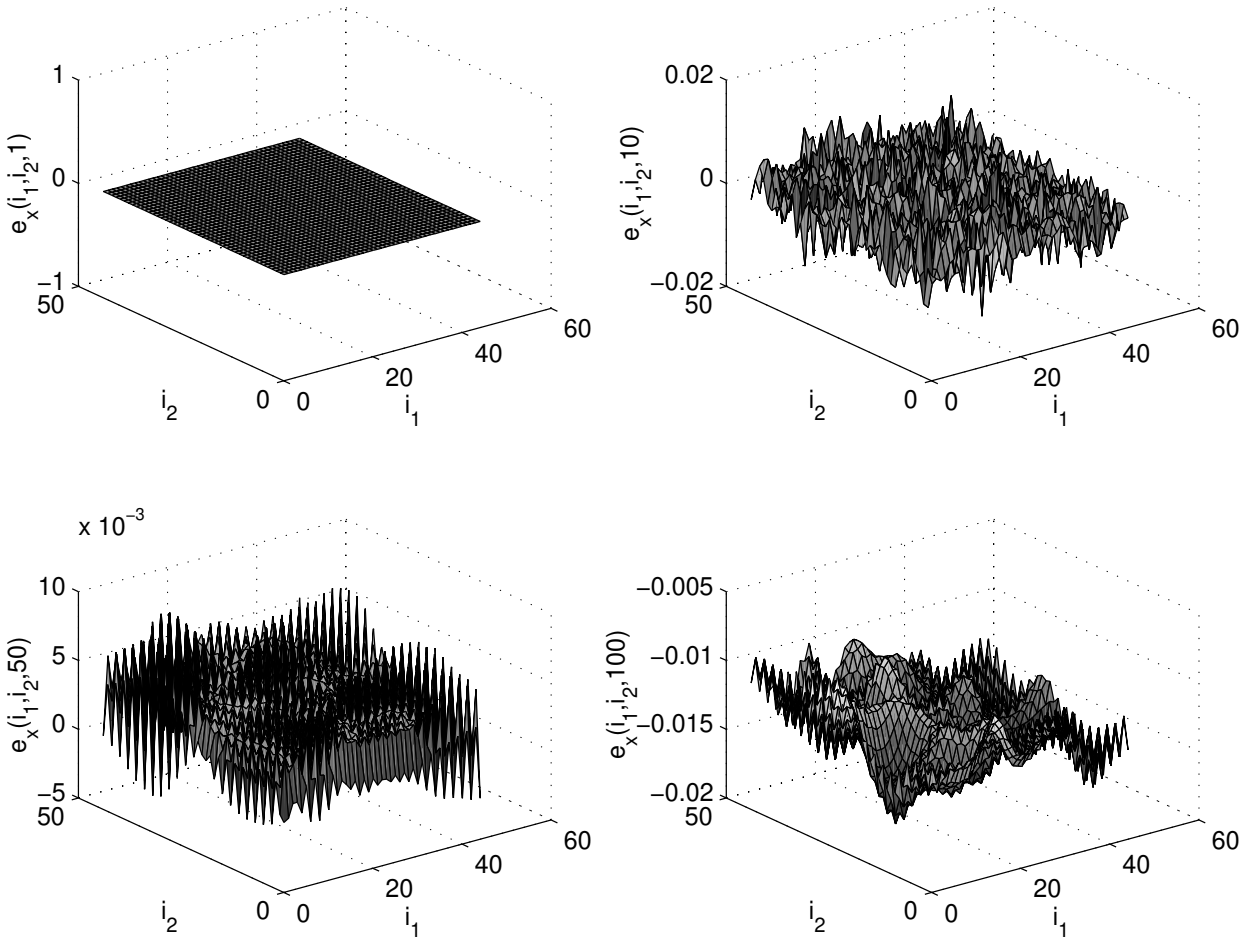

Figure 9: Example 2: Some snapshots of model predicted error (x)

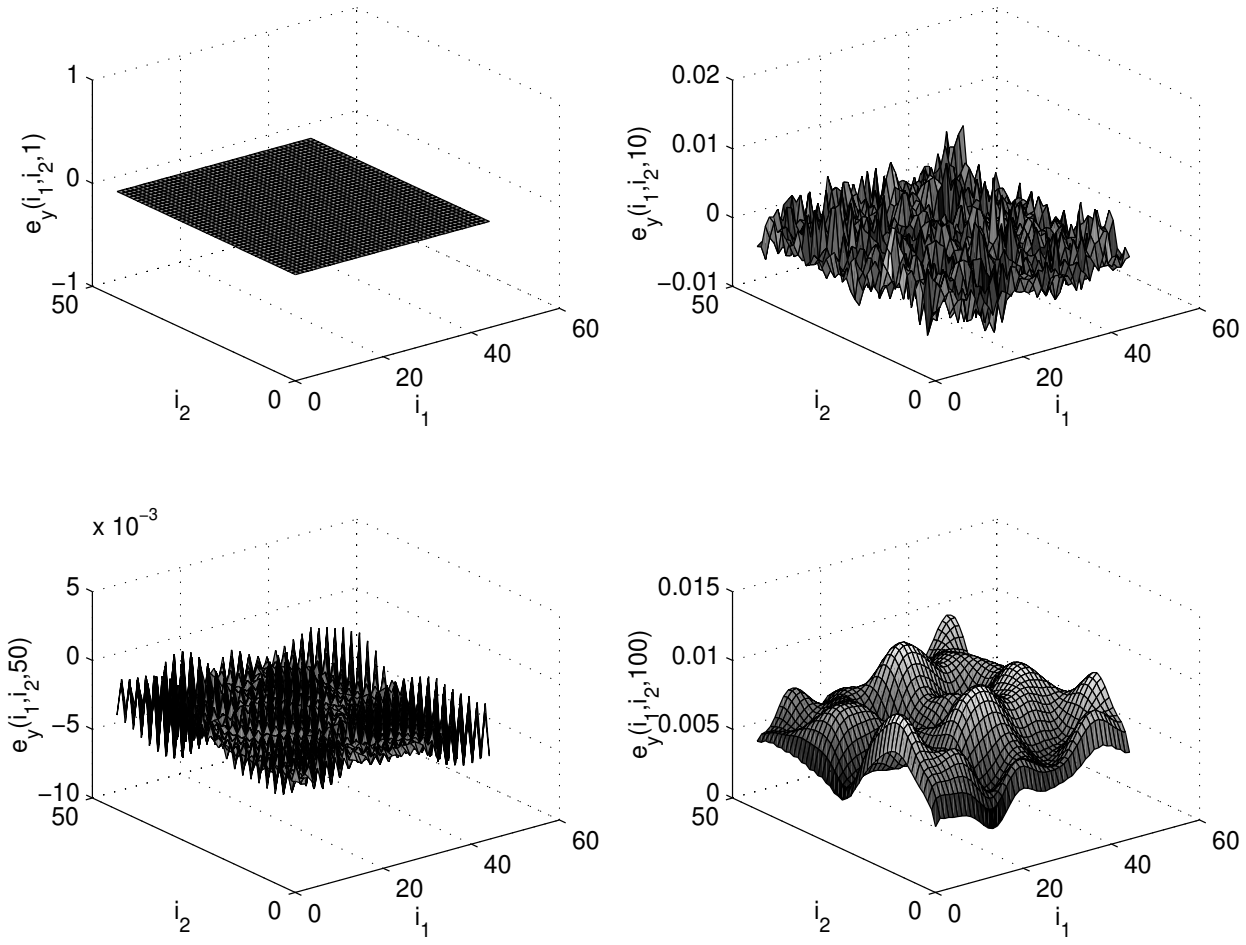

Figure 10: Example 2: Some snapshots of model predicted error (y)

$$\begin{aligned} \frac{\partial u}{\partial t} &= \frac{\partial^2 u}{\partial x^2} + \frac{\partial^2 u}{\partial y^2} - u^2 v \\ \frac{\partial v}{\partial t} &= \frac{\partial^2 v}{\partial x^2} + \frac{\partial^2 v}{\partial y^2} + u^2 v - k_1 v \end{aligned} \tag{29}$$

in which $-5 \leq x, y \leq 5$ and $k_1 = 0.5$, subject to the following initial conditions

$$u(x, y, 0) = 1; v(x, y, 0) = e^{-(x^2+y^2)} \tag{30}$$

and boundary conditions

$$\begin{aligned} u(5, y, t) &= u(x, 5, t) = u(-5, y, t) = u(x, -5, t) = 1 \\ v(5, y, t) &= v(x, 5, t) = v(-5, y, t) = v(x, -5, t) = 0 \end{aligned} \tag{31}$$

The linearise θ-method (Ramos 1997) was applied to solve the nonlinear PDEs (29) with parameters $\theta = 0.5, k = 0.05, h = H = 0.4, \alpha = \beta = 0.5$. Snapshots at time instants 1, 9, 10, and 11 are shown in Figs.(11) and (12). Note that all data were normalised to (0 1).

A set of 1000 observations randomly selected among the data set was used for identification. The identification was performed using the proposed method with the four nearest neighbours. The settings are same as those in example 2. The identified model is listed in Table (2)

Some snapshots of the model predicted outputs and the corresponding errors are plotted in Figs.(13), (14), (15), and (16), which show that the identified CML model can reproduce the spatio-temporal patterns of the original system very well. The RMS's for these snapshots are RMS(u,9) = 0.0041, RMS(u,10) = 0.0042, RMS(u,11) = 0.0045, RMS(v,9) = 0.0044, RMS(v,10) = 0.0055, RMS(v,11) = 0.0071, respectively.

6 Conclusions

A novel approach to the identification of CML models of spatio-temporal dynamics, which is the origin of some pattern formation phenomena, has been introduced. It has been demonstrated that the B-spline wavelet multiresolution approximation method provides a powerful approximation tool for the spatio-temporal dynamics being responsible for pattern formation. It is also shown that it is possible to extract the CML model using only a small number of spatio-temporal locations. Simulation results were included to demonstrate that the new wavelet-based identification procedure can produce excellent final CML models with a very good model predictive performance.

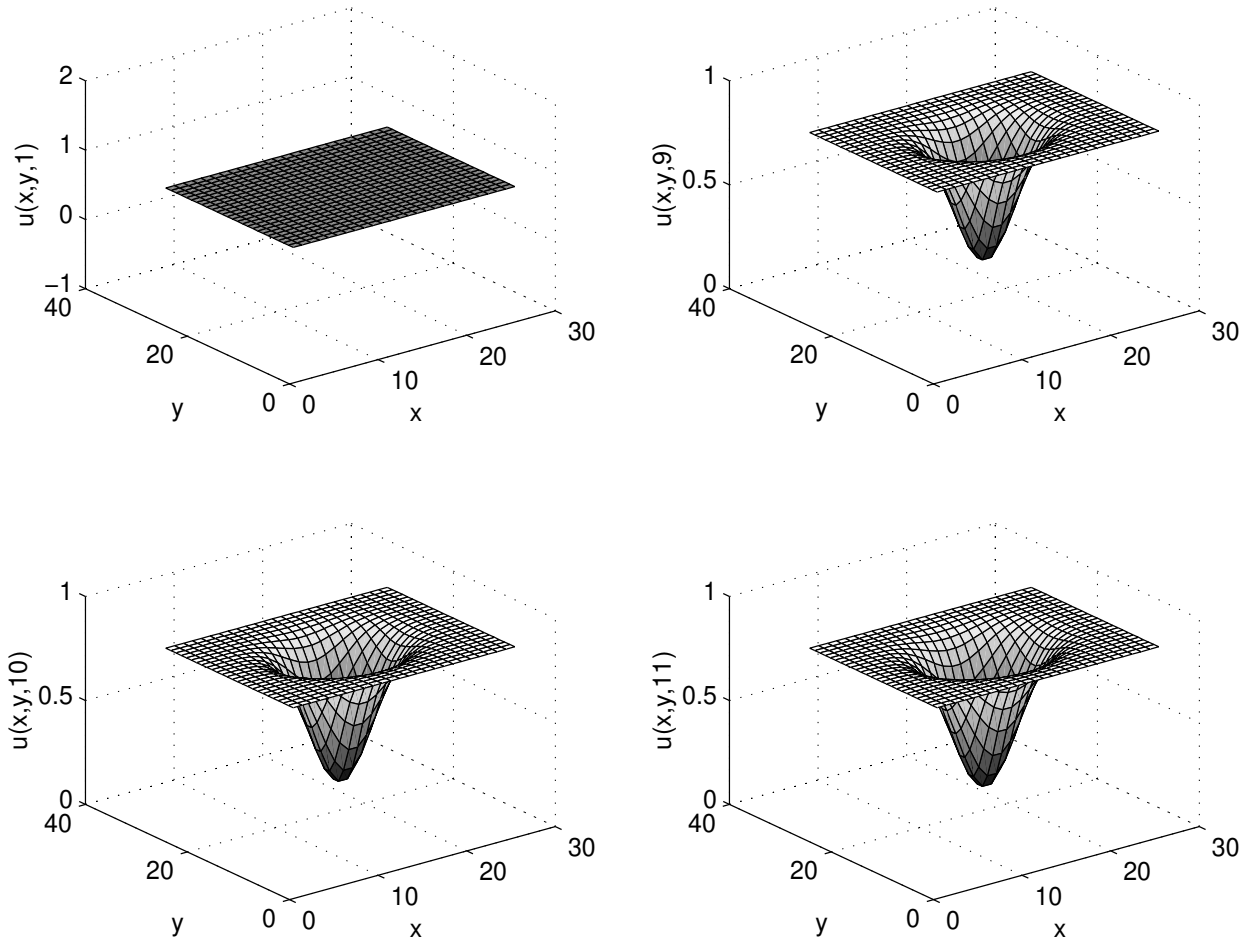

Figure 11: Example 3: Some snapshots of data (u)

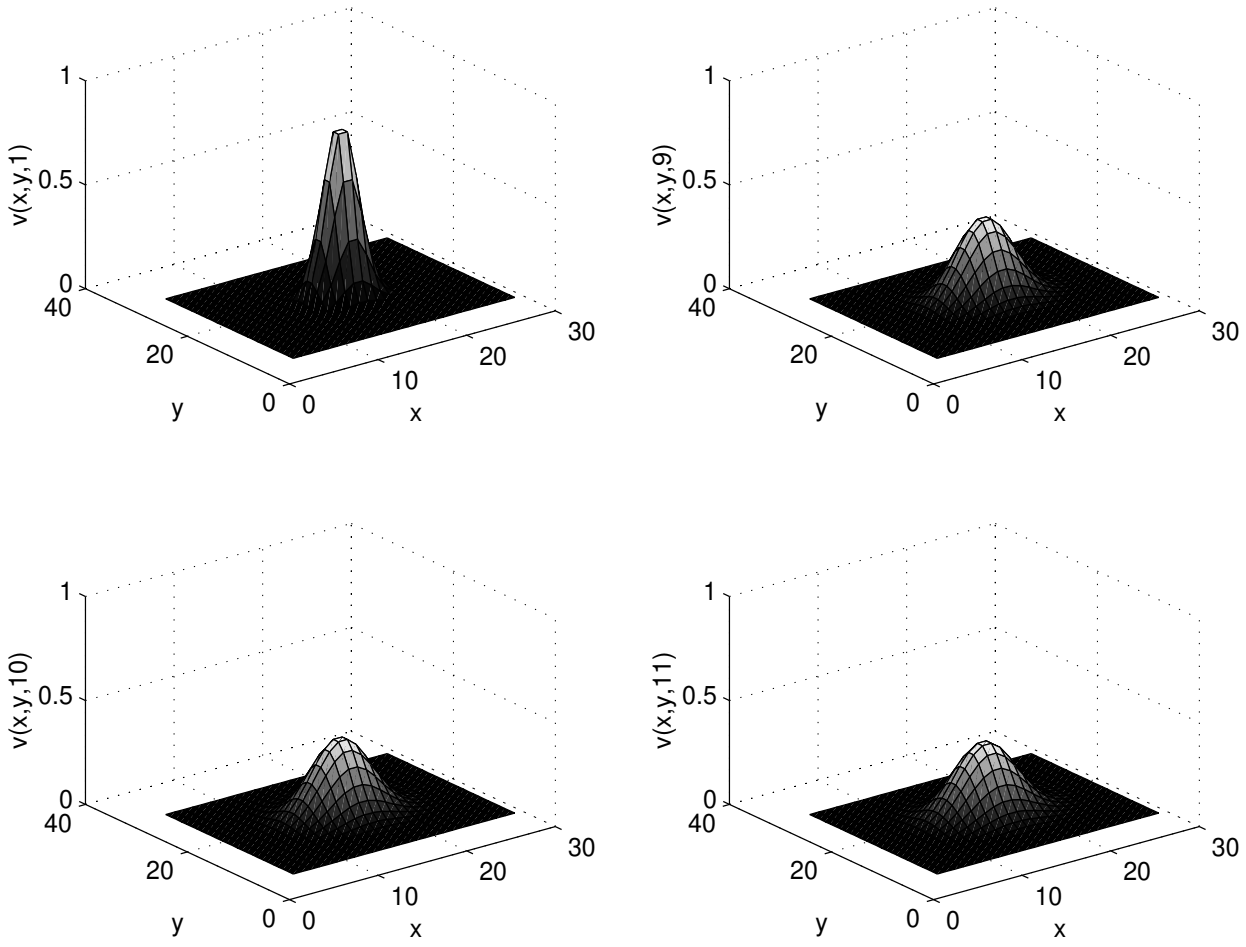

Figure 12: Example 3: Some snapshots of data (v)

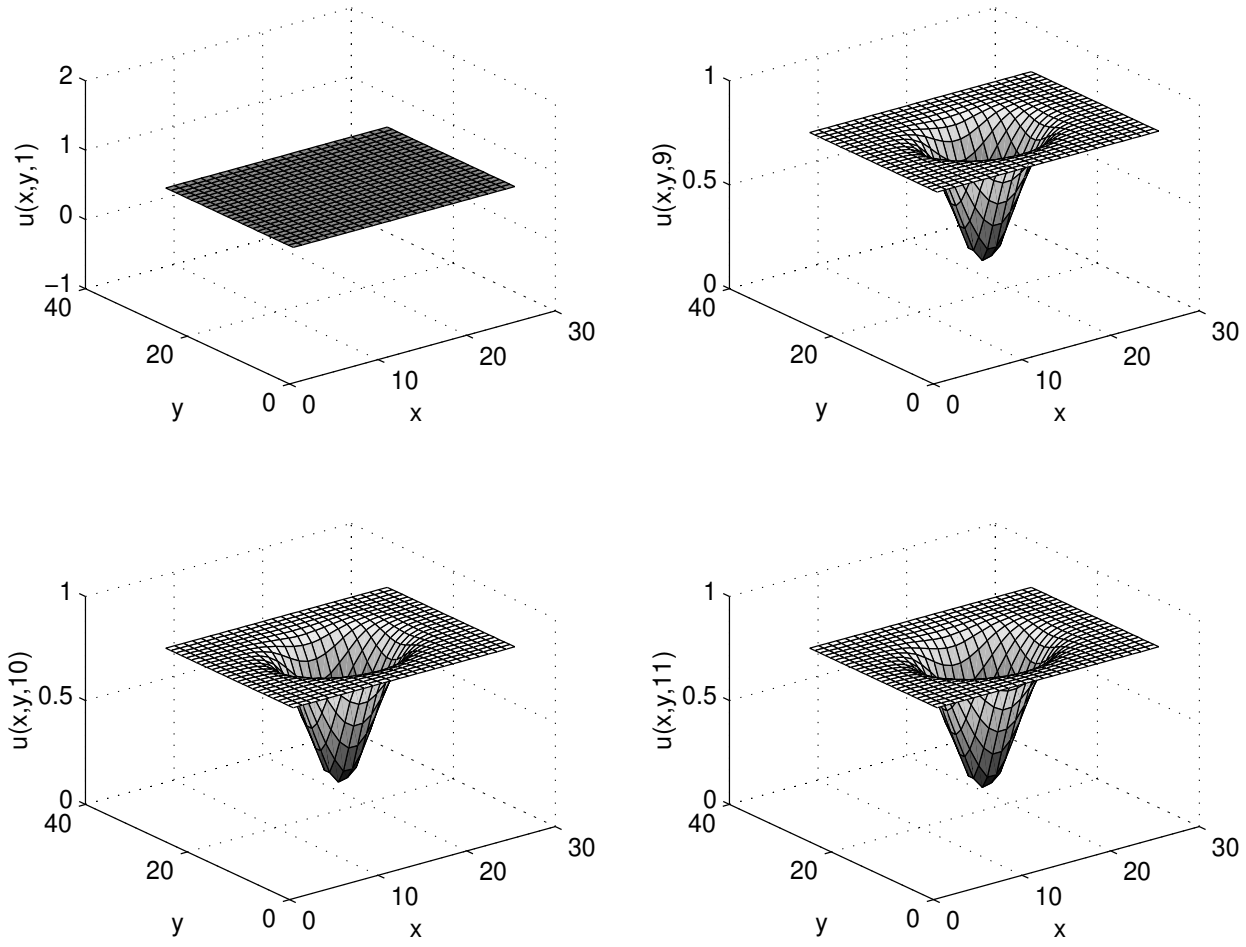

Figure 13: Example 3: Some snapshots of model predicted outputs (u)

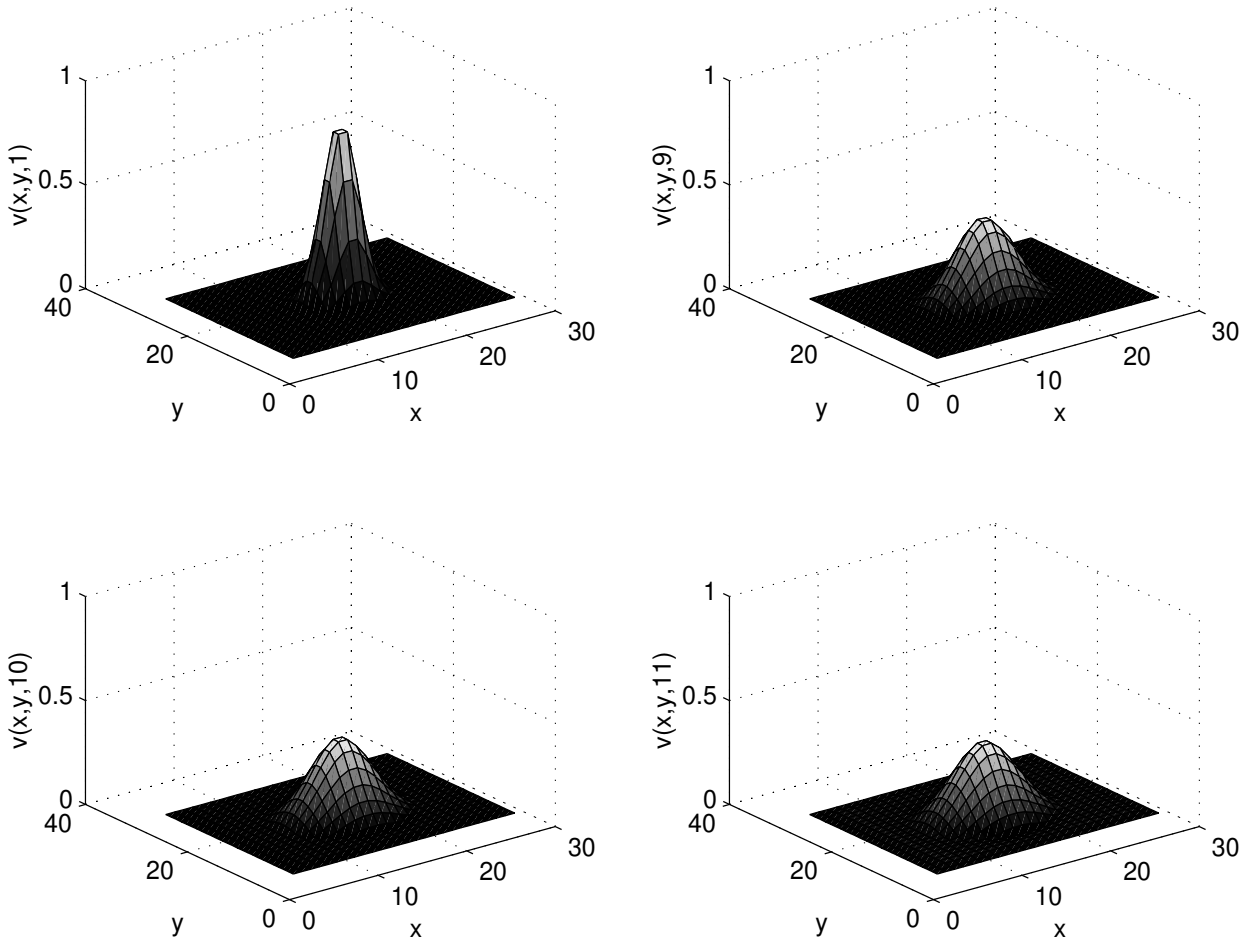

Figure 14: Example 3: Some snapshots of model predicted outputs (v)

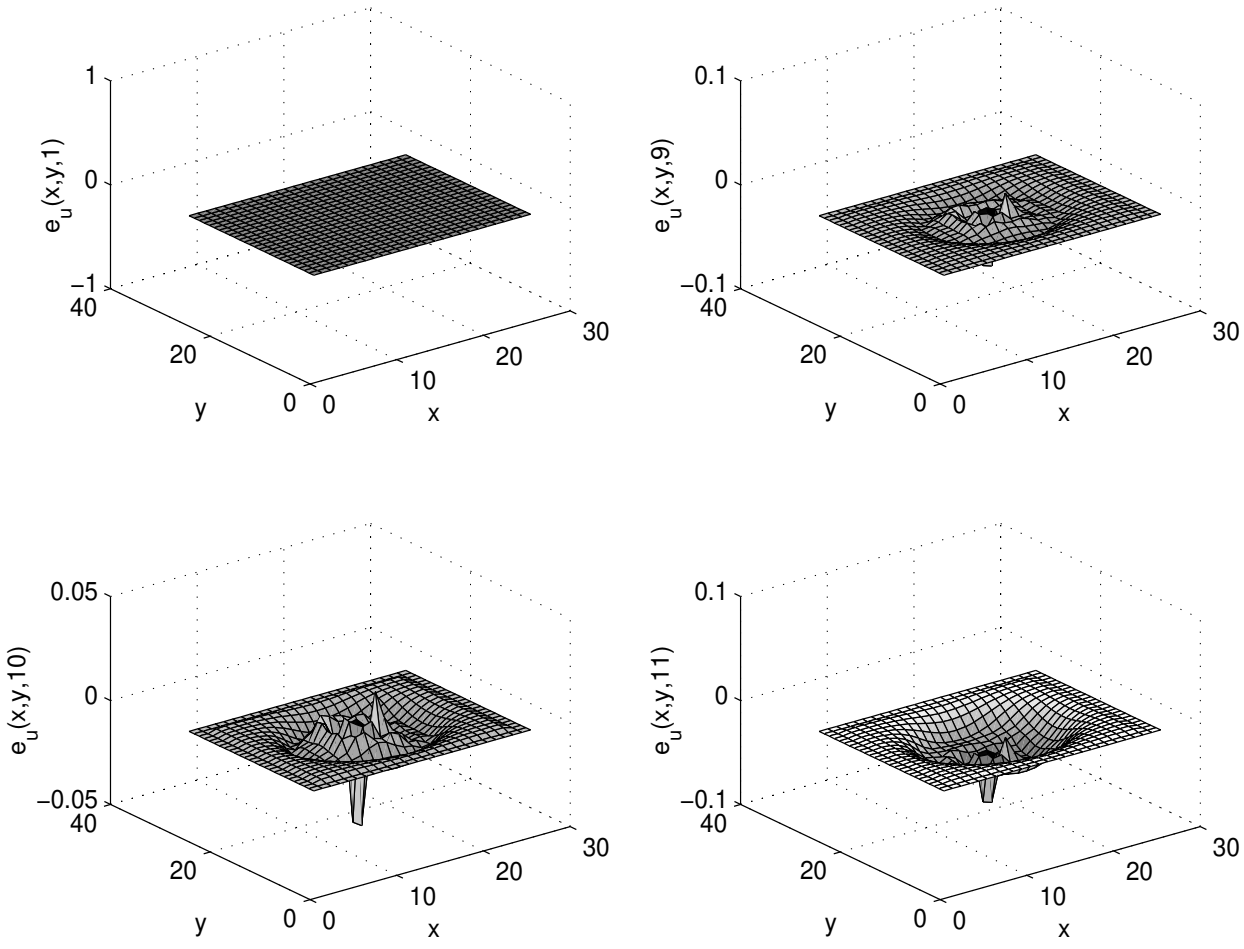

Figure 15: Example 3: Some snapshots of model predicted error (u)

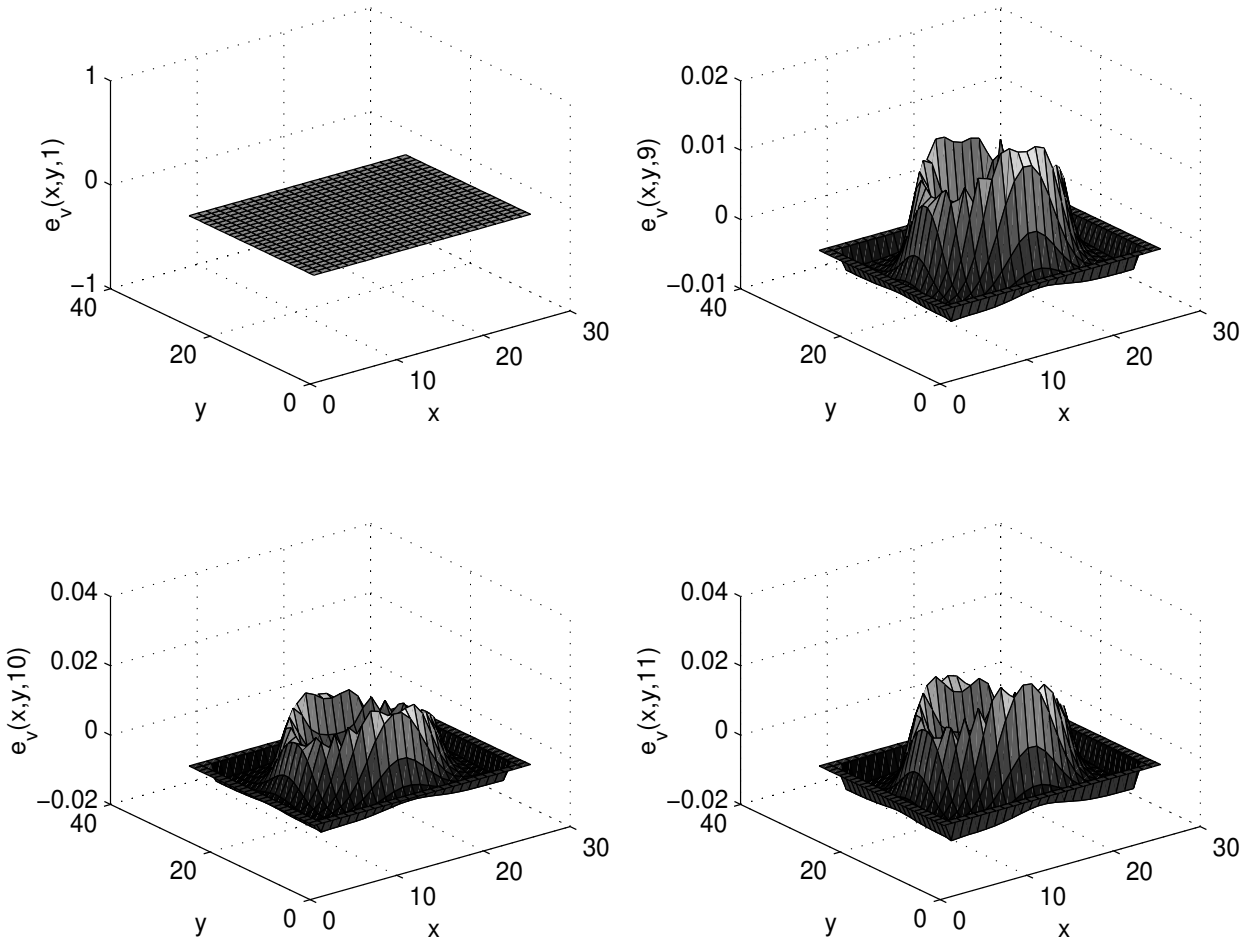

Figure 16: Example 3: Some snapshots of model predicted error (v)

7 Acknowledgement

The authors gratefully acknowledge financial support from EPSRC (UK).

References

[1] Adamatzky, A., (2003) On patterns in affective media, *International Journal of Modern Physics C*, Vol. 14, No. 5.

[2] Bertram, M., Beta, C., Pollmann, M., Mikhailov, A. S., Rotermund, H. H., and Ertl, G., (2003) Pattern formation on the edge of chaos: experiments with CO oxidation on a Pt(110) surface under global delayed feedback, *Phys. Rev.*, E67, No. 3, 036208.

[3] Billings, S. A. and Coca, D., (2002) Identification of coupled map lattice models of deterministic distributed parameter systems, *Int. J. Systems Science*, Vol. 33, pp. 623-634.

[4] Billings, S. A., Wei, H. L., Mei, S. S., and Guo, L. Z., (2003) Identification of spatio-temporal systems using multiresolution wavelet models, *Research Report, The University of Sheffield.*

[5] Chen, S., Billings, S. A., and Luo, W., (1989) Orthogonal least squares methods and their application to non-linear system identification, *International Journal of Control*, Vol. 50, No. 5, pp. 1873-1896.

[6] Chui, C. K. and Wang, J. Z., (1991) A general framework of compactly supported splines and wavelets, *J. Approx. Theroy*, Vol. 71, pp. 263-304.

[7] Coca, D. and Billings, S. A., (2001) Identification of coupled map lattice models of complex spatio-temporal patterns, *Phys. Lett.*, A287, pp. 65-73.

[8] DeVore, R. A., Jawerth, B., and Popov, V., (1992) Compression of wavelet decompositions, *American Journal of Mathematics*, Vol.114, pp.737-785.

[9] Goldman, D. I., Shattuck, M. D., Sung, J. M., Swift, J. B., and Swinney, H. L., (2003) Lattice dynamics and melting of a nonequilibrium pattern, *Phys. Rev. Lett.*, Vol. 90, No. 10, 104302.

[10] Grabec, I. and Mandelj, S., (1997) Continuation of chaotic fields by RBFNN, in *Biological and Artificial Computation: From Neuroscience to Technology: Proc.*, Mira, J. et al. eds., Lecture Notes in Computer Science, Springer-Verlag, Vol. 1240, pp. 597-606.

[11] Guo, L. Z., Mei, S. S., and Billings, S. A., (2002) Neighbourhood detection and identification of spatio-temporal dynamical systems using a coarse-to-fine approach, *Research Report, The University of Sheffield*, No. 828.

[12] He, G., Cao, L., and Li, J., (1995) Convective coupled map for simulating spatiotemporal chaos in flows, *Acta Mechanica Sinica*, Vol. 11, pp. 1-7.

[13] Kaneko, K., (1985) Spatio-temporal intermittency in couple map lattices, *Progress of Theoretical Physics*, Vol. 74, No. 5, pp. 1033-1044.

[14] Kaneko, K., (1986) Tuebulence in coupled map lattices, *Physica*, D18, pp. 475-476.

[15] Kaneko, K., (1989a) Spatiotemporal chaos in one- and two-dimensional coupled map lattices, *Physica*, D37, pp. 60-82.

[16] Kaneko, K., (1989b) Pattern dynamics in spatiotemporal chaos: pattern selection, diffusion of defect and pattern competition intermittency, *Physica*, D34, pp. 1-41.

[17] Kaneko, K. (eds.), (1993) *Coupled map lattice: theory and experiment*, World Scientific, Singapore.

[18] Köhler, P., Reinhard, K., and Huth, A., (2002) Simulating anthropogenic impacts to bird communities in tropical rain forests, *Biological Conservation*, Vol. 108, pp. 35-47.

[19] Mandelj, S., Grabec, I., and Govekar, E, (2001) Statistical approach to modeling of spatiotemporal dynamics, *Int. J. Bifurcation & Chaos*, Vol. 11, No. 11, pp. 2731-2738.

[20] Marcos-Nikolaus, P., Martin-Gonzalez, J. M. and Sóle, R. V., (2002) Spatial forcasting: detecting determinism from single snapshots, *Int. J. Bifurcation and Chaos*, Vol. 12, No. 2, pp. 369-376.

[21] Mei, S. S., Billings, S. A. and Guo, L. Z., (2004) A neighbourhood selection method for cellular automata models, *Int. J. Bifurcation and Chaos*, in press.

[22] Parlitz, U. and Merkwirth, C., (2000) Prediction of spatiotemporal time series based on reconstructed local states, *Phys. Rev. Lett.* , Vol. 84, No. 9, pp. 2820-2823.

[23] Platt, N. and Hammel, S., (1997) Pattern formation in driven coupled map lattices, *Physica*, A239, No. 1-3, pp. 296-303.

[24] Ramos, J. I., (1997) Linearization methods for reaction-diffusion equations: multi-dimensional problems, *Applied Mathematics and Computation*, Vol. 88, Nos. 2-3, pp. 225-254, 1997.

[25] Sóle, R. V., Valls, J. and Bascompte, J., (1992) Spiral waves, chaos and multiple attactors in lattice models of interacting populations, *Phys. Lett.*, A166, No. 2, pp. 123-128.

[26] Sweldens, W. and Piessens, R., (1994) Asymptotic error expansion of wavelet approximations of smooth function II, *Numerische Mathematik*, Vol. 68, No. 3, pp. 377-401.

[27] Tabuchi, E., Yakawa, T., Mallick, H., Inubushi, T., Kondoh, T., Ono, T., and Torii, K., (2002) Spatio-temporal dynamics of brain activated regions during drinking behaviour in rats, *Brain Research*, Vol. 951, pp. 270-279.

[28] Yanagita, T., (1992) Phenomenology of boiling: a coupled map lattice model, *Chaos*, Vol. 2, No. 3, pp. 343-350.

[29] Yanagita, T. and Kaneko, K, (1997) Modeling and characterisation of cloud dynamics, *Phys. Rev. Lett.*, Vol. 78, No. 22, pp. 4297-4300.

Output	Terms	Estimates	ERR	STD
$x_{i_1,i_2}(t)$	constant	3.8433e-01	8.7610e-01	1.4077e-01
	$\psi_{2,2}(y_{i_1,i_2}(t-1))$	-1.2124e-01	9.6519e-02	6.6171e-02
	$\psi_{1,0}(x_{i_1+1,i_2}(t-1))$	7.6028e-02	1.8084e-02	3.8552e-02
	$\phi_{0,0}(y_{i_1,i_2}(t-1))$	-4.7015e+00	5.7288e-03	2.3874e-02
	$\psi_{2,2}(x_{i_1,i_2}(t-1))$	9.3786e-02	1.9155e-03	1.6236e-02
	$\psi_{2,0}(x_{i_1,i_2+1}(t-1))$	2.7505e-03	5.6392e-04	1.3169e-02
	$\psi_{1,1}(x_{i_1,i_2+1}(t-1))\psi_{1,0}(y_{i_1,i_2}(t-1))$	6.9983e-02	3.6318e-04	1.0740e-02
	$\phi_{0,0}(x_{i_1,i_2+1}(t-1))\phi_{0,0}(x_{i_1-1,i_2}(t-1))\phi_{0,0}(y_{i_1,i_2}(t-1))$	2.4546e+01	1.7859e-04	9.3155e-03
	$\psi_{1,1}(x_{i_1,i_2}(t-1))$	2.0974e-01	1.4123e-04	8.0119e-03
	$\phi_{0,0}(x_{i_1-1,i_2}(t-1))\psi_{0,0}(x_{i_1,i_2}(t-1))))\psi_{0,0}(x_{i_1,i_2+1}(t-1))$	1.6507e+01	1.5181e-04	6.3174e-03
	$\psi_{1,1}(x_{i_1,i_2}(t-1))\psi_{1,0}(y_{i_1,i_2}(t-1))$	-1.2217e+00	9.7807e-05	4.9261e-03
	$\phi_{0,0}(x_{i_1+1,i_2}(t-1))\psi_{0,0}(x_{i_1,i_2}(t-1))$	1.0330e+01	4.6795e-05	4.0966e-03
	$\phi_{0,0}(x_{i_1-1,i_2}(t-1))\phi_{0,0}(x_{i_1+1,i_2}(t-1))\phi_{0,0}(y_{i_1,i_2}(t-1))$	-8.9812e+01	3.9069e-05	3.2456e-03
	$\psi_{1,0}(x_{i_1,i_2}(t-1))\psi_{1,1}(x_{i_1+1,i_2}(t-1))$	-1.6302e-01	1.2889e-05	2.9107e-03
	$\psi_{1,0}(x_{i_1+1,i_2}(t-1))\psi_{1,1}(y_{i_1,i_2}(t-1))$	3.6020e-02	2.2595e-05	2.2042e-03
	$\psi_{0,0}(x_{i_1,i_2}(t-1))\psi_{0,0}(x_{i_1+1,i_2}(t-1))$	3.1263e+01	5.4336e-06	1.9974e-03
	$\psi_{1,0}(x_{i_1+1,i_2}(t-1))\psi_{1,0}(y_{i_1,i_2}(t-1))$	1.1940e+00	2.7952e-06	1.8821e-03
	$\psi_{1,0}(x_{i_1,i_2+1}(t-1))\psi_{1,1}(x_{i_1-1,i_2}(t-1))$	6.2831e-02	2.9436e-06	1.7526e-03
	$\psi_{2,3}(y_{i_1,i_2}(t-1))$	1.7394e+00	1.8794e-06	1.6647e-03
	$\psi_{2,-1}(y_{i_1,i_2}(t-1))$	1.6716e-01	4.0256e-06	1.4585e-03
$y_{i_1,i_2}(t)$	$\psi_{0,0}(x_{i_1,i_2}(t-1))$	1.3139e+00	8.9932e-01	7.0977e-02
	$\phi_{0,0}(y_{i_1-1,i_2}(t-1))$	1.5873e+00	9.4832e-02	1.8130e-02
	$\psi_{2,1}(y_{i_1,i_2-1}(t-1))$	1.0295e-02	2.3593e-03	1.4117e-02
	$\psi_{1,1}(y_{i_1,i_2-1}(t-1))\psi_{1,0}(y_{i_1-1,i_2}(t-1))$	5.7969e-01	1.5581e-03	1.0518e-02
	$\phi_{0,0}(y_{i_1,i_2+1}(t-1))\phi_{0,0}(x_{i_1,i_2}(t-1))$	-1.0133e+00	4.1977e-04	9.2611e-03
	$\psi_{1,1}(y_{i_1,i_2}(t-1))$	-1.1484e-01	5.8458e-04	7.2940e-03
	$\psi_{2,1}(y_{i_1-1,i_2}(t-1))$	5.9592e-03	2.0760e-04	6.4294e-03
	$\psi_{1,0}(y_{i_1,i_2}(t-1))\psi_{1,1}(y_{i_1+1,i_2}(t-1))$	4.3107e-01	1.4600e-04	5.7438e-03
	$\phi_{0,0}(x_{i_1,i_2}(t-1))$	4.2620e-01	1.1322e-04	5.1450e-03
	$\psi_{1,1}(y_{i_1,i_2}(t-1))\psi_{1,0}(x_{i_1,i_2}(t-1))))$	3.1168e-01	1.1049e-04	4.4891e-03
	$\psi_{1,1}(y_{i_1-1,i_2}(t-1))\psi_{1,0}(y_{i_1+1,i_2}(t-1))$	-2.9189e-01	1.2308e-04	3.6253e-03
	$\phi_{0,0}(y_{i_1,i_2+1}(t-1))$	6.9789e-01	4.3826e-05	3.2642e-03
	$\phi_{0,0}(y_{i_1,i_2}(t-1))\phi_{0,0}(x_{i_1,i_2}(t-1))$	3.4402e+01	2.4669e-05	3.0406e-03
	$\psi_{2,-1}(y_{i_1,i_2}(t-1))$	-7.1065e-01	4.8533e-05	2.5431e-03
	$\psi_{1,0}(x_{i_1,i_2}(t-1))$	2.3366e-01	3.5731e-05	2.1040e-03
	$\psi_{2,2}(y_{i_1+1,i_2}(t-1))$	1.7527e-02	3.0430e-05	1.6391e-03
	$\psi_{1,0}(y_{i_1,i_2}(t-1))\psi_{1,0}(x_{i_1,i_2}(t-1))$	1.7527e-02	3.0430e-05	1.6391e-03
	$\psi_{2,2}(y_{i_1,i_2+1}(t-1))$	1.5146e-02	9.7495e-06	1.0354e-03
	$\psi_{1,0}(y_{i_1,i_2+1}(t-1))\psi_{1,0}(y_{i_1+1,i_2}(t-1))$	9.1224e-01	4.5186e-06	9.0215e-04
	$\phi_{0,0}(y_{i_1,i_2}(t-1))\phi_{0,0}(y_{i_1,i_2-1}(t-1))\phi_{0,0}(y_{i_1,i_2+1}(t-1))$	4.3590e+01	4.5071e-06	7.4578e-04

Table 2: Example 2: The terms and parameters of the final CML model

Output	Terms	Estimates	ERR	STD
$u_{i_1,i_2}(t)$	$\phi_{0,0}(u_{i_1,i_2}(t-1))$	1.8150e+00	9.9456e-01	6.0566e-02
	constant	1.5719e-01	5.0708e-03	1.6284e-02
	$\psi_{0,0}(u_{i_1,i_2}(t-1))$	1.3661e+00	2.1655e-04	1.0551e-02
	$\phi_{0,0}(u_{i_1-1,i_2}(t-1))\phi_{0,0}(u_{i_1+1,i_2}(t-1))\phi_{0,0}(v_{i_1,i_2}(t-1))$	-2.8209e+00	9.6277e-05	6.5501e-03
	$\psi_{1,1}(u_{i_1,i_2}(t-1))$	5.5517e-02	2.6212e-05	4.9273e-03
	$\phi_{0,0}(u_{i_1,i_2}(t-1))\psi_{0,0}(u_{i_1,i_2-1}(t-1))\psi_{0,0}(u_{i_1,i_2+1}(t-1))$	6.9926e+00	2.3658e-05	2.7328e-03
	$\psi_{1,0}(u_{i_1,i_2-1}(t-1))\psi_{1,0}(v_{i_1,i_2}(t-1))$	-2.8170e-02	3.2177e-06	2.2764e-03
	$\psi_{1,1}(v_{i_1,i_2}(t-1))$	-1.2303e-02	1.8597e-06	1.9648e-03
	$\phi_{0,0}(v_{i_1,i_2}(t-1))$	-2.0857e-01	9.9731e-07	1.7754e-03
	$\psi_{2,2}(v_{i_1,i_2}(t-1))$	-2.2390e-02	1.6544e-06	1.4059e-03
	$\phi_{0,0}(u_{i_1-1,i_2}(t-1))\phi_{0,0}(u_{i_1+1,i_2}(t-1))$	4.7945e-01	9.8767e-07	1.1290e-03
	$\psi_{2,2}(u_{i_1,i_2}(t-1))$	6.1474e-02	9.5835e-07	7.7053e-04
$v_{i_1,i_2}(t)$	$\psi_{0,0}(v_{i_1,i_2}(t-1))$	5.2401e+00	7.5727e-01	4.6122e-02
	constant	1.3540e-01	2.2576e-01	2.1066e-02
	$\psi_{2,2}(v_{i_1,i_2}(t-1))$	8.9719e-02	1.1325e-02	1.2151e-02
	$\psi_{2,-1}(v_{i_1,i_2}(t-1))$	1.5265e-01	3.7064e-03	7.1220e-03
	$\psi_{1,-1}(v_{i_1-1,i_2}(t-1))\psi_{1,-1}(v_{i_1+1,i_2}(t-1))$	7.3020e+01	1.0890e-03	4.7164e-03
	$\psi_{2,0}(v_{i_1,i_2}(t-1))$	-3.4268e-02	3.7021e-04	3.5445e-03
	$\psi_{2,3}(v_{i_1,i_2}(t-1))$	-2.5037e+00	1.3663e-04	2.9984e-03
	$\psi_{0,0}(u_{i_1,i_2}(t-1))$	-1.0459e-01	1.4235e-04	2.2952e-03
	$\psi_{2,-2}(v_{i_1,i_2}(t-1))$	-6.2861e-01	1.2632e-04	1.4016e-03
	$\phi_{0,0}(v_{i_1,i_2}(t-1))\phi_{0,0}(u_{i_1,i_2}(t-1))$	3.3724e-01	4.3742e-05	9.0593e-04
	$\psi_{0,0}(v_{i_1,i_2-1}(t-1))\psi_{0,0}(v_{i_1-1,i_2}(t-1))\psi_{0,0}(u_{i_1,i_2}(t-1))$	7.7240e+00	8.0454e-06	7.8123e-04
	$\psi_{1,0}(u_{i_1,i_2}(t-1))$	-5.7745e-03	3.6728e-06	7.1713e-04
	$\phi_{0,0}(u_{i_1,i_2}(t-1))$	2.6142e-02	4.2205e-06	6.3554e-04
	$\phi_{0,0}(v_{i_1,i_2-1}(t-1))\phi_{0,0}(v_{i_1,i_2+1}(t-1))$	1.0843e+01	3.0703e-06	5.6887e-04
	$\phi_{0,0}(v_{i_1,i_2}(t-1))\phi_{0,0}(v_{i_1,i_2-1}(t-1))\phi_{0,0}(v_{i_1,i_2+1}(t-1))$	2.3366e-01	3.5731e-05	2.1040e-03
	$\psi_{2,2}(y_{i_1+1,i_2}(t-1))$	-3.8382e+01	1.6023e-06	5.3077e-04

Table 3: Example 3: The terms and parameters of the final CML model